Progress in Natural Science: Materials International xxx (xxxx) xxx

HOSTED BY

ELSEVIER

Contents lists available at ScienceDirect

Progress in Natural Science: Materials International

journal homepage: www.elsevier.com/locate/pnsmi

Chevrel phase: A review of its crystal structure and electrochemical properties

Meng Liu [a], Guocheng Lv [a,*], Tianming Liu [b], Hao Liu [b], Lingchang Kong [a], Lintao Tian [a], Wenxiu Rao [a], Yuxin Li [a], Libing Liao [a], Juchen Guo [c,d]

[a] Engineering Research Center of Ministry of Education for Geological Carbon Storage and Low Carbon Utilization of Resources, Beijing Key Laboratory of Materials Utilization of Nonmetallic Minerals and Solid Wastes, National Laboratory of Mineral Materials, School of Materials Science and Technology, China University of Geosciences (Beijing), 100083, China

[b] School of Science, China University of Geosciences, Beijing, 100083, China

[c] Materials Science and Engineering Program, University of California - Riverside, Riverside, CA, 92521, United States

[d] Department of Chemical and Environmental Engineering, University of California – Riverside, CA, 92521, United States

ARTICLE INFO

Keywords:
Chevrel phase
Electrochemical properties
Energy storage
Electro-catalysis

ABSTRACT

Chevrel phase compounds have attracted increasing attention as electrochemical energy storage materials and electro-catalysts. Benefiting from their unique crystal structure, Chevrel phase compounds can not only function as the host structures for reversible intercalation of a broad range of cations, but also exhibit high catalytic activity in electrochemical reduction reactions. Here we provide an overview of recent progress in the development of Chevrel phase materials including new understanding of structural features, synthetic methods, and electrochemical properties. A brief conclusion and perspectives on the future development of Chevrel phase materials are also provided.

1. Introduction

Energy efficiency is a global issue that requires effective and environmentally benign energy conversion and storage technologies to achieve carbon neutralization by 2050 [1]. Electrochemical energy storage systems and electrocatalytic energy conversion and production are among the new technologies attracting significant research and development efforts in the past decades. Chevrel phase compounds are a group of inorganic materials that can play important roles in the field of electrochemical energy storge and electro-catalysis due to their unique crystal structure and properties. Crystal structures of Chevrel phase are well established [2], and their general formula can be described as $M_nMo_6X_8$, where M is a cation that can be alkali metal, alin earth metal, transition metal, or rare earth elements such as Pb, Sn, Cu, Ag, Zn et al., n is the content of M elements, and X is S, Se, Te or combinations of these elements with I and Br [3]. Recently, interests in Chevrel phase compounds have been increasing with new understanding of their properties and discovery of their potential applications involving electrochemistry. In this review, we focus on the latest progress in electrochemical applications combining the battery technique and catalytic aspects of Chevrel phase compounds by discussing their structural tunability, novel synthetic method, and electrochemical properties as illustrated in Fig. 1.

2. Crystal structure and properties

Chevrel phase is characterized by hexagonal rhombic symmetry (space group R3), while there is triaxial deformation (space group P1) or advanced cluster aggregation (space group $P6_3/m$) in which m elements are small cations [4]. These phases can be described as a stack of Mo_6X_8 cluster cells, and each of the cell is a slightly twisted cube. Chalcogen atoms are located at the corners and molybdenum atoms are located at the center of the plane [5]. All the Mo atoms and six chalcogen atoms are located in 6f positions, the other two sulfur group atoms are located at the 2c positions on the triaxial axis. Each Mo atom in Mo_6 octahedral cluster is surrounded by five sulfur group atoms and constitutes a square pyramid. The bottom of the pyramid is actually the surface of the Mo_6X_8 cell, and the top is the sulfur group atom belonging to the neighboring Mo_6X_8 unit [6]. There are two kinds of anions in Chevrel: including X_1 which is on the ternary axis and X_2 which is on the general position, as shown in Fig. 2. The quasi-rigid Mo_6X_8 cell network is separated by three-dimensional chalcogen channels. The channels can host many guest cations in two quasi-cubic chalcogenide cavities [7]. The crystal structure of Mo_6S_8 is illustrated in Fig. 2, cavity 1, the so-called “inner sites” is located in the origin of the rhombic cell with point symmetry3 (000) formed by 8 sulfur group atoms belonging to 8 different Mo_6X_8

* Corresponding author.
E-mail address: guochenglv@cugb.edu.cn (G. Lv).

https://doi.org/10.1016/j.pnsc.2023.01.002
Received 18 November 2022; Received in revised form 7 January 2023; Accepted 18 January 2023
Available online xxxx

Please cite this article as: M. Liu et al., Chevrel phase: A review of its crystal structure and electrochemical properties, Progress in Natural Science: Materials International, https://doi.org/10.1016/j.pnsc.2023.01.002

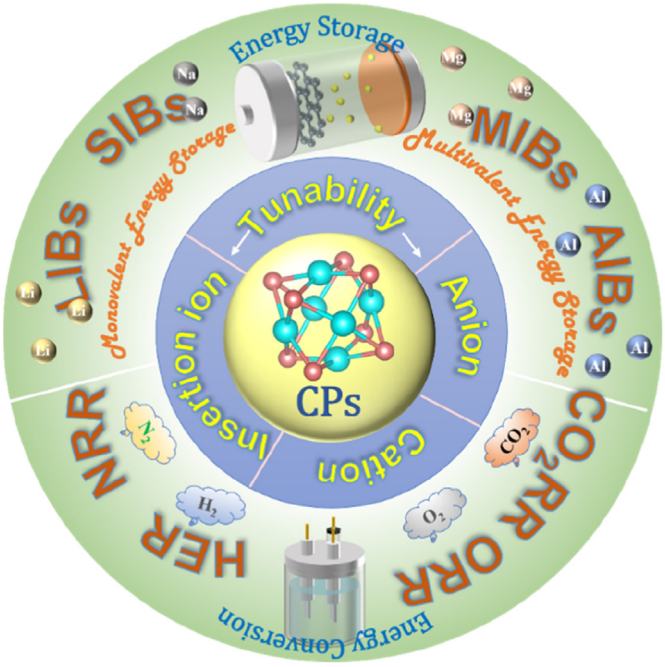

Fig. 1. Schematic diagram of the electrochemical applications of Chevrel phase compounds.

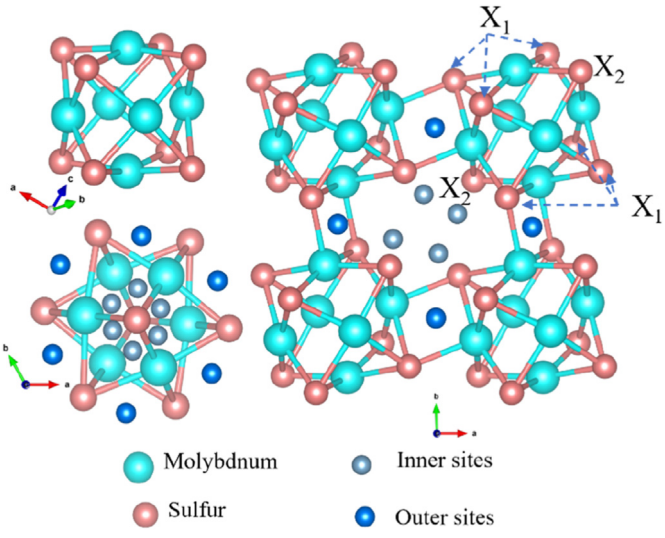

Fig. 2. Crystal structure of Mo_6S_8.

units. Cavity 2, the so-called "outer sites" is located between the rhombic axis ($\bar{1}$ point symmetrical) and formed from eight sulfur group atoms belonging to four different Mo_6X_8 units. Cavity 2 shares a pseudo square plane opposite the other two cavities 1 along the rhombic axis (1/200) (01/20) (001/2) [8]. Compared to cavity 2, cavity 1 is more likely to be accessible by foreign cations, which helps to explain the off-stoichiometry of Chevrel phase compounds [9].

As alluded above, the crystal structure of Chevrel phase with open framework and connected channels enables intercalation of guest cations with high cation mobility. Each Mo_6 cluster is able to accept up to four electrons to accommodate the cation insertion. These crystal structure properties combined with high electronic conductivity makes Chevrel phase compounds excellent candidates as rechargeable battery cathode materials. Crystal structures of CPs are very flexible and all components of the ternary phase can be replaced with multiple elements [10]. The flexibility of CPs is described in the following sections. They also find applications in electrocatalysis: the electronic structure and the corresponding catalytic properties of Chevrel phase compounds such as charge transport and binding energy with intermediates can be tuned via foreign ion intercalation, cation and anion substitution. Furthermore, different Chevrel phase structures can provide diverse chemical environments that can alter the reaction pathways.

Chevrel phase compounds are the only group of materials capable rapid and reversible intercalation of various cations including monovalent (Li^+, Na^+, and Cu^+), divalent (Zn^{2+}, Cd^{2+}, Ni^{2+}, Mn^{2+}, Co^{2+} and Mg^{2+}) and even trivalent (Al^{3+}) [11–13]. Moreover, the insertion of an M cation into metal-containing CPs, $M'_xMo_6X_8$, which may cause a displacement reaction associated with the M + M′ cation motion in the crystal structure. Chevrel phase compounds can be generally divided into two main structural groups, classic and new, by cation sequence, In the classic Chevrel phase, cavity 1 is firstly occupied, and the inserted cation may be at its origin or with a little shift from the origin. In the new Chevrel phase, the intercalated cation may occupy cavity 2 due to the repulsion interactions between intercalated cation and Mo atoms. The arrangements and kinds of intercalated cations can be affected by the symmetry and structure types. Such as, the phases present triclinic when intercalated by Cr, Mn, Ti, and Fe; the phases present trigonal with Co and Ni intercalating. The research has shown [11] that during the insertion of the bigger cations (such as, Na, Ag, Sn and Pb) in the classic Chevrel phase, the delocalization of cations decreases the chemical bond of M-X. among which Na^+ demonstrated the lowest delocalization among all guest cations. The intercalated big cations are only movable on the surface of the CP's structure. It is worth noting that when the insertion force is high enough, the cations can be movable inside the structure.

Meanwhile the anion and cation of Mo framework can be substituted. In the structure of CPs, anions (S^{2-}, Se^{2-}, etc.) showed high ordered sequences. The rhombic structure of Chevrel phase consists of a slightly twisted cubic block of Mo_6X_8 where eight anions are located at the cube angle. Six Mo cations are arrayed in octahedral geometry. Anions occupy distinct sites: X_1 and X_2 as illustrated in Fig. 2. S anion in the structure can be substituted by Se and Te anions. When the radius of intercalated cation is more than 1 Å, S prefers to occupy X_1 site, while the intercalated cation is smaller or no cation is intercalated, Se prefers to occupy X_1 site. The order of anions can be affected by difference anion sizes [14]. And the Mo atom can be entirely or partially substituted by other transition metals. Meanwhile there are many interests in the study of pseudo-ternary compounds. In the binary Mo_6X_8 phases molybdenum may be substituted with rhenium, rhodium, or ruthenium, partially [15]. The unit cell volume of these compounds was lower than the Mo_6X_8 binary compound, and the possibility of insertion of Ru and Rh into Mo_6 cluster outside structure such as $M_xMo_6X_8$ compounds was eliminated. The primary difference between the lattice parameters of CPs is that the rhombohedral angel can be increased significantly, which may result in different physicochemical property. Such as CPs of $Mo_4Ru_2Se_8$ is semiconducting while the CPs of $Mo_4Ru_2Te_8$ and $Mo_{4.66}Rh_{1.33}Te_8$ present the property of metal [16].

3. Synthesis of Chevrel phase compounds

Chevrel phase was synthesized by Chevrel et al. for the first time in the year of 1971 [17]. In contrast to the selenide and telluride binary compounds, binary sulfides are metastable and cannot be synthesized from directly combining the two elements. However, it can be produced by deintercalation of the ternary phase [18]. The preparation methods of Mo_6X_8 can be typically categorized into high-temperature solid state synthesis (HT), two-step solution chemistry method (TSC), molten salt synthesis (MSS) method, and other novel synthesis methods, including high energy mechanical milling method (HEMM), Swagelok type reactors (STR) method, and microwave synthesis method (MSM). It is worth mentioning that machine learning has been used to guide the synthesis of Chevrel phase compounds [19]. Different aspects of the

synthesis methods are discussed below including single crystal Chevrel phase synthesis.

The most common synthesis technique to obtain the ternary $M_xMo_6S_8$ Chevrel compounds is to sinter the mixture of corresponding elements of M, Mo, and S in an evacuated quartz tube for several days at temperatures between 400 and 1200 °C. The particle size of the synthesized compounds is no more than 0.2 mm, even after long time annealing at 1200 °C [20,21]. As aforementioned, binary Mo_6Se_8 and Mo_6Te_8 can be synthesized directly by sintering the mixture of Mo and Se or Te [22,23]. To eliminated native oxides, the elemental precursors need to be reduced in H_2 first [24]. The calcination usually takes several days at a temperature between 800 and 1200 °C [25].

Ternary Chevrel sulfides can also be synthesized from sulfide precursors soluble in organic solvents. Stoichiometric ratio of ammonium tetrathiomolybdate and anhydrous copper chloride were dissolved in N,N-Dimethylformamide (DMF) under N_2 atmosphere. The reactant was heated to 90 °C for a period, which was filtered, and following tetrahydrofuran was added to the filtrate to initiate precipitation, which was kept overnight. The products were washed by tetrahydrofuran and methanol followed by drying and annealing under Ar and H_2 gas mixture atmosphere [26–28]. However, pretreatment procedure and the introduction of H_2 may be the bottleneck of this method [29]. To improve the reaction kinetics, molten salts were studied as the medium for the synthesis of ternary Chevrel compounds using the Mo chalcogenide, elemental Mo, and copper chalcogenide precursors. The system was reacted under a slow flow of Ar at 850 °C for 60 h. The products need to be washed thoroughly by deionized water to remove the salts. Lower temperature and shorter duration can be achieved by the molten salt methods without stringent requirement of inert environment [30].

More efficient methods to synthesize ternary Chevrel compounds have been demonstrated using precursors composed of stoichiometric ratio of Mo chalcogenide, elemental Mo, and copper chalcogenide. For instance, MoS_2 (or $MoSe_2$), Mo, CuS (or CuSe) were well mixed under high-speed ball milling and pressed into pellets and gradually heated to 800–1100 °C for a several hours under Ar [7,31,32]. Swagelok reactor was used to synthesize $Cu_{2.5}Mo_6S_{8-n}Se_n$ (n = 0,1,2) using the mixture of the same precursors without pressing into pellets [33]. Instead of conventional heating, microwave method recently demonstrated significant reduction of reaction time. Carbon is introduced in the microwave synthesis to absorb radiation and prevent the oxidation of precursors. The thermal treatment can be reduced to 400 s under the power of 1200 W by laboratory microwave [34]. The abovementioned synthetic methods of Chevrel phase have been summarized in Table 1.

Synthesizing single crystal Chevrel compounds is very important to study the intrinsic properties of the materials. To date, the common method to grow single crystal Chevrel compounds is Stockberger-Bridgman technique [35]. Single crystal can be prepared by heating the mixture of precursors at 1200–1800 °C (to the melting point) for a period, and the cooling procedure needs to be slow enough to promote crystallization [36,37]. For instance, the size of $FeMo_6Se_8$ single crystals can reach 0.5–1 mm^3 [38].

Table 1
Summary of regular synthetic methods in Chevrel phase.

Synthetic method	Temperature	Atmosphere	Merit and demerit	Ref.
HT	400–1200 °C	vacuum	long duration	20–25
TSC	90 °C	hydrothermal	hydrogen is required during secondary calcination	26–29
MSS	850 °C	Ar	molten salt volatilization	30
HEMM	800–1100 °C	Ar	introducing ball milling	7, 31-32
STR	900 °C	Ar	introducing vessel	33
MSM	microwave 1200 W	Ar	security issue	34

The binary Chevrel compounds can be derived from the parent ternary structure by removing the cations from the inner and outer sites. It is typically achieved by chemical leaching. Different oxidizing agents such as HCl, I_2 and NO_2BF_4 are used. The binary Chevrel compounds can be obtained by using different oxidizing agents such as 6 M HCl in water and 0.2 M I_2 or 0.05 M NO_2BF_4 in acetonitrile under air or O_2 atmosphere [39].

4. Applications of Chevrel compounds

4.1. Energy storage applications

Rechargeable batteries, with low cost and high abundant reserves, have been promising candidates for energy storage and conversion. Although lithium-ion batteries achieve commercialization, the uneven distribution in crust of lithium resources has become bottleneck of development. Due to the natural abundance and uniform distribution of other metal on earth, the post lithium-ion (such as Na, Mg, Al and K) battery has developed rapidly [40,41]. Nevertheless, there many factors that can affect the battery performance, such as lower conductivity, low ion diffusivity, sluggish interfacial/surface transfer kinetics, and volume expansion. While, CPs has the properties of high electroconductibility and high ionic mobility, which enables preferable electrochemical performance. The binary Chevrel compounds with vacated inner and outer sites have been studied and demonstrated as electrode materials for secondary batteries because of their rich crystal structural cavities to host ion intercalation. Nagao et al. carried out a series of studies on Chevrel compounds as anode materials for Li-ion batteries [42]. Lu et al. have recently proposed a strategy to stabilize Li metal anode using artificial solid electrolyte interphase (SEI) composed of Mo_6S_8 and carbon. Direct contact of Mo_6S_8 and Li in the presence of electrolytes resulted in rapid diffusion of Li ions into Mo_6S_8 crystal structure, resulting in formation of Li intercalated Mo_6S_8. The Mo_6S_8-stabilized Li anode paired with $LiNi_{0.8}Mn_{0.1}Co_{0.1}O_2$ cathode demonstrated significantly improved cycle stability compared with pristine Li anode [43]. A Li-ion battery with high-concentration aqueous water-in-salt electrolyte was demonstrated with Mo_6S_8 anode and $LiMn_2O_4$ cathode, delivering outstanding cycling performance and high Coulombic Efficiency (CE) [44]. Aurbach's group also proposed an energy storage device composed of battery-supercapacitor Mo_6S_8/Ti_3C_2 hybrid negative electrode and carbon positive electrode in high-concentration aqueous electrolytes. It was found that 14 M LiCl solution was an excellent electrolyte providing the wide electrochemical window up to 2.7 V, which is superior to 21 M bistrifluoromethanesulfonimide lithium salt (LiTFSI) aqueous solution [45]. Elgendy et al. recently reported a full aqueous battery which is comprised of nano Mo_6S_8 anode and $LiMn_2O_4$ cathode with 21 M LiTFSI as electrolyte. The crystal structure of the Mo_6S_8 anode was well sustained after demonstrating excellent cycling stability [46]. In-situ X-ray absorbtion spectra method was used to reveal the local structure of Mo_6S_8 during Li^+ electrochemical insertion. The results suggest that Li^+ ions intercalate in Mo_6S_8 with five stages and de-intercalate with four. Most stages are assigned to two-phase transition reactions. However, systematic investigations are needed by combining other operando technologies such as NMR and XRD to correlate the change in the local structure to the electrochemical properties [47].

Mo_6S_8 was studied by Yue et al. as the cathode material in and an all-solid-state sodium ion battery (SIB). Na_3PS_4 solid electrolyte (SE) was coated on Mo_6S_8 cathode to improve the contact between cathode and SE. Such modification enabled a SIB with a high cycling performance of 500 cycles maintaining capacity of 52 mAh/g [48]. Similar to the artificial SEI composed of Mo_6S_8 for Li metal anode, Mo_6S_8 was also studied as the key component in the artificial SEI to stabilize Na metal anode by Lu et al. [49]. $Na_xMo_6S_8$ SEI film was in situ synthesized and the coated Na anode demonstrated improved stability than the pristine Na electrode.

Chevrel compounds have been extensively investigated as cathode

materials for rechargeable Mg-ion batteries (MIBs), which were first reported by Aurbach et al. in 2000 [50]. Reversible Mg^{2+} cation intercalation in Mo_6S_8 was demonstrated in electrolytes based on Mg organohaloaluminate complex [50]. Notably, guest Mg atoms can locate in the channels between Mo_6S_8 blocks with feature of delocalization, in which there are 12 possible positions for Mg atoms, while only some of the sites can be occupied due to geometrical and electrostatic limitations. This work established Chevrel compounds, particularly Mo_6S_8, as the benchmark cathode materials for rechargeable Mg-ion batteries. Following, there are many researches about CPs electrode material in recent years. As shown in Fig. 3 (a), a stable Mg ion battery comprised of Mg and Mo_6S_8 was carried out with capacity of 70 mAh/g for 200 cycles at C/5 rate. And the rate performance can be improved by adding of carbon nano tube (CNT) in cathode [51]. Yu et al. has revealed the charge distribution on S of CPs during Mg insertion in Fig. 3 (b). The S in CPs displays different valence state with nonuniform charge distribution. When the cation is inserted, the charge distribution becomes uniform, which is related to chemical stability and electrochemical reversibility. Structure evolution is attributed to the bond length change by the delocalization of inserted cations [52]. As CPs was deemed to the most stable cathode materials for multivalent batteries, it is also used as benchmarking cathode material so as to investigate other parts in the battery.

In recent work, a novel non-nucleophilic IL-based electrolyte was developed in Mg ion battery. The battery displays high stability remaining 80% capacity over 300 cycles in the full cell with Mo_6S_8 cathode [53]. Aurbach et al. proposed the study of the role of surface adsorbed Cl^- in rechargeable Mg ion battery. The research described the role of Cl^- in intercalation process of Mg ions into CPs. It was found that the addition of Cl^- to electrolyte, or pretreatment of CPs in chloride containing solutions could promote reversible Mg intercalation with fast kinetics [54]. It has been found that CPs modified separator can effectively improve the shuttling issue in Mg–S battery in Fig. 3(c and d). Remarkably, the Mg–S cell assembled by CPs modified separator can achieve a high specific energy density of 942.9 mAh/g in the 1st cycle and the CE can be attained to 96% at 0.2C for 200 cycles. It is also found that the energies needed to separate the cation and anion at CP are much lower than carbon surface, which facilitates the conversion reaction [55]. Kang et al. have synthesized different crystalline structures $Cu_xMo_6S_8$ (Cu-CP) by varying the temperature and time, which were used as precursors for Mo_6S_8 cathodes. It was found that the discharge capacities can be improved from 84.2 to 122.9 mAh/g as the structure of Cu-CP changed from rhombohedral to triclinic in Fig. 3 (e). In general, the electrochemical Mg insertion occurs in two stages, formatting new phases with $Mg_1Mo_6S_8$ and $Mg_2Mo_6S_8$ as rhombohedral, which can be

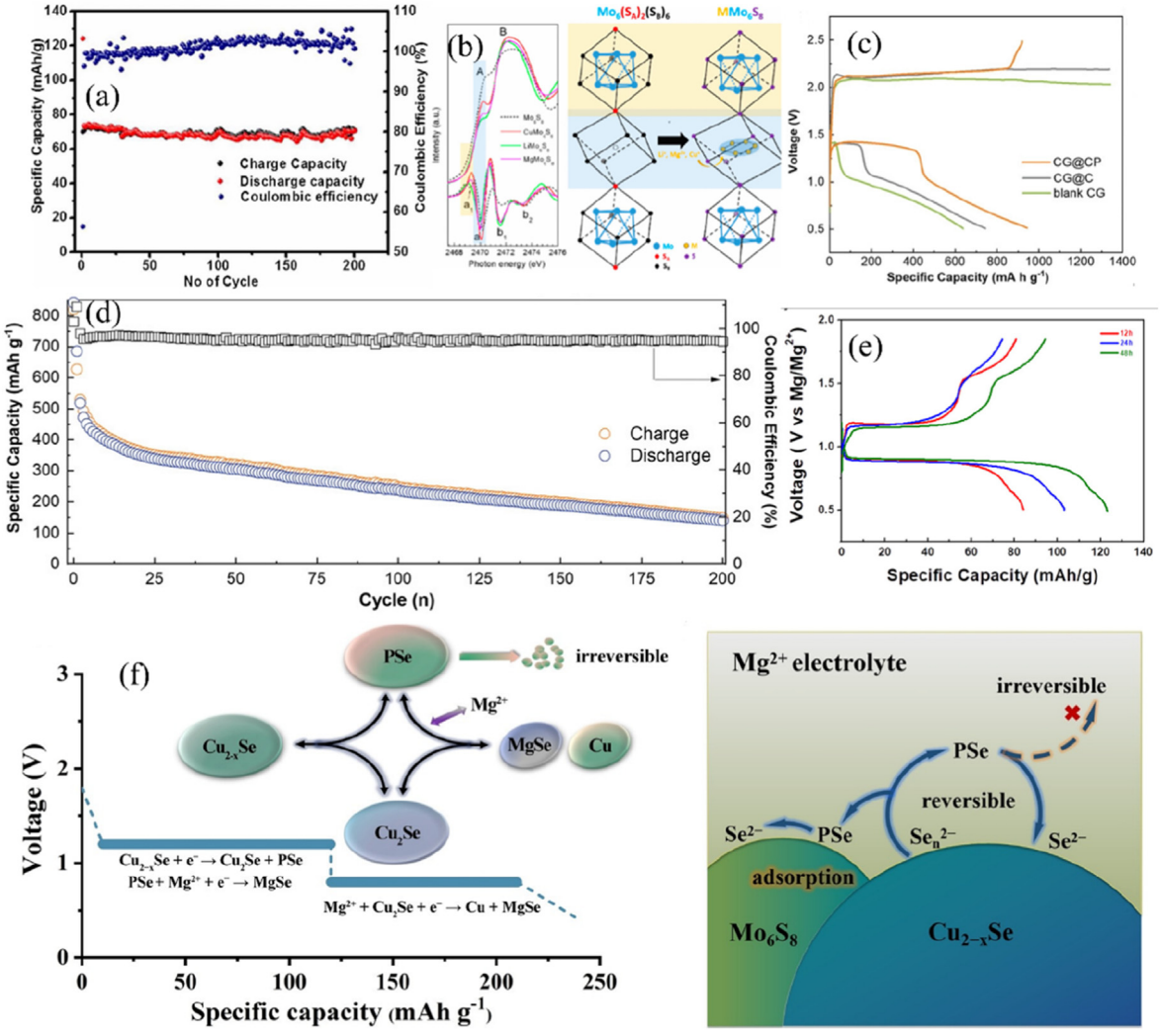

Fig. 3. (a) Cycling stability of Mo_6S_8 in Mg ion battery [51]; (b) Absorption spectra of the S K-edge and crystal structure change for $CuMo_6S_8$, $LiMo_6S_8$, and $MgMo_6S_8$ [52]; (c) Galvanostatic discharge/charge performance of Mg–S cells; (d) Long cycling performance of Mg–S cells with CG@CPs at 0.2C [55]; (e) Electrochemistry of the Mo_6S_8 cathode coin cell at room temperature [56]; (f) The schematic diagram of the Mg^{2+}-storage mechanism of the $Cu_{2-x}Se$ cathode and intercalation-conversion hybrid cathode [57].

described as the following eqs (1) and (2) [56]:

$$Mg^{2+}+2e^{-}+Mo_6S_8 \rightarrow Mg_1Mo_6S_8 \quad (1)$$

$$Mg^{2+}+2e^{-}+Mg_1Mo_6S_8 \rightarrow Mg_2Mo_6S_8 \quad (2)$$

Qu et al. introduced Mo_6S_8 into $Cu_{2-x}Se$ cathode to immobilize polyselenide so as to retard the dissolution issue. As shown in Fig. 3 (f), it was found that adding of Mo_6S_8 can significantly improve the reversible capacity from 140 mAh/g to 220 mAh/g [57]. It also found that halogen-free Mg^{2+}/Li^{+} dual salting containing gel-polymer electrolytes (GPE) using Mo_6S_8 as cathode and carbon coating $Mo_6S_8$for MIBs also play superior electrochemical performance [58,59].

Among the rechargeable batteries beyond Li-ion, Al ion batteries are particularly promising due to the high abundance of Al and the high theoretical capacity [60]. In 2015, Geng et al. first demonstrated the reversible Al intercalation in Mo_6S_8 with a prototype battery composed of an Al anode, a Mo_6S_8 cathode, and a Lewis acidic chloroaluminate ionic liquid electrolyte [61]. In 2018, the same group further elucidated the crystal structure transformation of Mo_6S_8 during Al ion intercalation. It is revealed that unlike the intercalation of monovalent and divalent cations, Al cations intercalate in Mo_6S_8 by equally occupying the inner and outer sites without preference due to the strong Al^{3+}-Al^{3+} repulsion, which illustrates the easy diffusion of Al^{3+} from body-center to face-center in Chevrel phase [62]. Mao et al. reported a method to synthesize Mo_6S_8 nanosheets, in which iodine was used to induce the preferential orientation. The Mo_6S_8 nanosheets were both applied in Mg and Al batteries, which shows fast kinetics, lower polarization, higher capacities and better electrochemical performance at lower temperature [31]. The same group of Suo recently has investigated the valence state evolution of CPs in aluminium ion batteries (AIBs). It revealed that S has been fully reduced, and Mo_6 cluster is firstly oxidized and then reduced with Al^{3+} insertion, which originated from the contraction and elongation of Mo–Mo bond in Mo_6 cluster [63]. The abovementioned performance of Chevrel phase cathode materials have been summarized in Table 2. Unlike other oxide cathode materials dissolving in Lewis acid, Mo_6S_8 can be stable in the Lewis acid electrolyte [64]. In order to understand the mechanism of the Al intercalation into Mo_6S_8, solid NMR method was used to understand quantitatively Al ion intercalation from molecular level. It is found that Al^{3+} in intercalate simultaneously into two kinds of cavities sites in CPs' framework during process discharge, which is consistent with the work of group Guo [62]. And cation trapping during deintercalation is lower than 7% [65]. The electrochemical redox equations during intercalating into two kinds of cavities are shown in eqs (3) and (4):

$$4Al_2Cl_7^{-}+3e^{-}+Mo_6S_8 \leftrightarrow AlMo_6S_8+7AlCl_4^{-} \quad (3)$$

$$4/3Al_2Cl_7^{-}+e-+AlMo_6S_8 \leftrightarrow Al_{4/3}Mo_6S_8+7/3AlCl_4^{-} \quad (4)$$

Table 2
Summary of performance in Chevrel phase cathode materials.

Cathode materials	Voltage/V	Specific capacity mAh/g	Battery type	Ref.
Mo_6S_8	~1.0–1.3	77	MIBs	50
Mo_6S_8/CNT	~1.1	75	MIBs	51
Mo_6S_8	~0.9	85	MIBs	53
Mo_6S_8	~0.8	70	MIBs	54
Mo_6S_8	~1.5–2.1	150	MIBs	55
Triclinic $CuMo_6S_8$	~1.1	122.9	MIBs	56
$Mo_6S_8/Cu_{2-x}Se$	~0.9–1.2	220	MIBs	57
Mo_6S_8	~1.3	80	MIBs	58
Mo_6S_8@C	~1.1	90	MIBs	59
Mo_6S_8	~0.37–0.55	70	AIBs	61
Mo_6S_8	~0.35–0.52	105	AIBs	62
Mo_6S_8	~0.4–0.55	160	AIBs	63

Interestingly, CPs also has been used as Janus material for energy generation and storage. Mo_6S_8 can be used in a combined device that assembles with an Al ion battery and a solar cell where Mo_6S_8 serves as the cathode and $Al_{4/3}Mo_6S_8$ serves as a solar absorber material with lower band gap [66].

4.2. Electro-catalysis applications

Chevrel compounds have also be investigated for electro-catalysis applications due to the high tunability of their electronic structures, which is rare in other group of materials.

A hollow nanostructure of $Ni_2Mo_6S_8$ synthesized by a template-directed route was one of the early Chevrel phase electrocatalysts used for hydrogen evolution reaction (HER) in alkaline electrolyte. This catalyst demonstrated good HER performance with a low overpotential of −257 mV to reach the current density of 10 mA/cm^2 as shown in Fig. 4 (a). There are about 20 electrons in the cluster of Mo_6S_8, offering a pool of charges that is beneficial for electrocatalytic reaction. And it has confirmed that Ni et al. transition metal can promote the HER performance by coupling with S to optimize the hydrogen adsorption strength [67]. It was also discovered that Mo_6S_8 exhibited excellent catalytic properties for HER in different electrolytes with a wide pH range including 0.5 M H_2SO_4, 0.1 M KOH, and 3% NaCl. The overpotentials vs. RHE are 0.32, 0.49 and 0.52 V, respectively in Fig. 4 (b), to reach current density of 10 mA/cm^2. The band structure of Mo_6S_8 is extremely narrow and consists of primarily Mo-4d and S-3d orbitals. Meanwhile, the metallic conductivity of Mo_6S_8, which suggests that the adsorption sites for hydrogen can be enhanced leading to higher HER performance [68]. Perryman et al. compared the electrocatalytic property of $M_2Mo_6S_8$ (M = K, Rb, and Cs) nanorods for HRE. $K_2Mo_6S_8$ is the most effective electrocatalyst for HER among all. It demonstrated a low overpotential of 270 mV to achieve a current density of 10 mA/cm^2 in 0.5 M H_2SO_4, whereas the overpotentials of $Rb_2Mo_6S_8$ and $Cs_2Mo_6S_8$ in the same condition were 349 and 328 mV, respectively [69]. The electrocatalytic properties of Mo_6X_8 (X = S, Se, Te) were studied with combined experimental and theoretical approach. Mo_6S_8 exhibited the lowest overpotential of 321 mV at 10 mA/cm^{-2} comparing with 432 and 634 mV vs RHE for Mo_6Se_8 and Mo_6Te_8, respectively. It is found that higher electronegativity of the anion framework increases the hydrogen adsorption strength and the Lewis basicity as shown in Fig. 4 (c). The Tafel slopes of Mo_6S_8, Mo_6Se_8 and Mo_6Te_8, ranging from 74 to 82 mV dec^{-1} indicating the rate-limiting step is electrochemical desorption as part of the Volmer−Heyrovsky mechanism [70]. Strachan et al. have prepared Mo_6X_8 nanoparticles with diameter less than 100 nm as electrocatalysts for hydrogen evolution. Nano Mo_6S_8 compared to bulk Mo_6S_8 significantly improved the HER performance by reducing the overpotentials from 0.67 V to 0.23 V vs. RHE at 10 mA/cm^2 due to the higher surface area. And after 1000 cycles, there was no significant change in the polarization curve of nano Mo_6S_8 [71]. Elgendy et al. also studied nanoscale Mo_6S_8 for HER in acidic media, which exhibited a promising and stable electrocatalytic activity with and overpotential at 264 mV vs SHE [72]. Recently, a mechanically-stable, all-metal, and highly active $CuMo_6S_8$/Cu electrode has been constructed with an overpotential of 172 mV at 10 mA/cm^2. What's even more remarkable is that a very small overpotential of 334 mV at a large current density of 2500 mA/cm^2 for over 100 h has been achieved which is of great significance in industrial application [73].

In addition to HER, Chevrel compounds are also studied for other electrochemically catalyzed reactions. $Cu_2Mo_6S_8$ was also found to be a good electrocatalysts for CO_2 reduction reaction (CO_2RR) to reduce CO_2 to CO under an overpotential of 0.4 V in aqueous condition vs SHE. Moreover, by selectively reduce the CO target molecule, it succeeded in suppressing the competing formic acid pathway and produced methanol as the only liquid phase product [75], which displays excellent product selectivity. Inspired by MoFe nitrogenase, $Fe_2Mo_6S_8$ was studied as nitrogen reduction reaction (NRR) electrocatalyst. The catalyst exhibited a

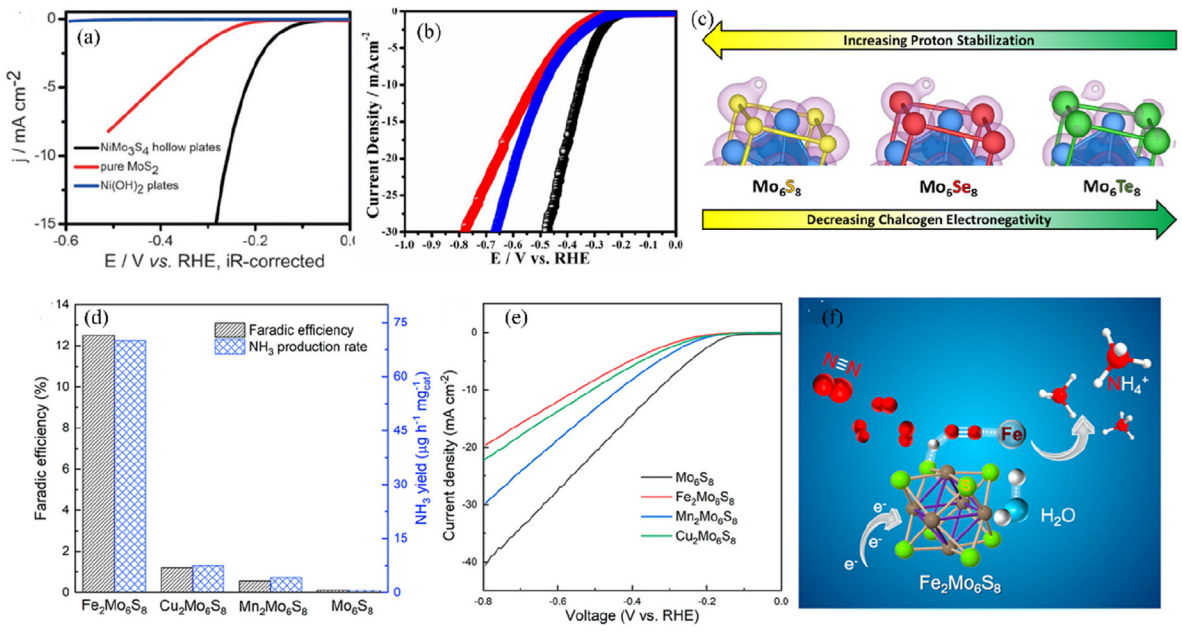

Fig. 4. (a) HER performance of hollow $NiMo_3S_4$ nanoplates and pure MoS_2 and $Ni(OH)_2$ nanoplates [67]; (b) HER performance of Mo_6S_8 in different electrolytes (Black: 0.5 M H_2SO_4, Red: 0.1 M KOH and Blue: 3% NaCl) [68]; (c) Function of electronegativity of anion framework and HER properties [70]; (d) Comparison of N_2 to NH_3 conversion efficiency and average NH_3 production rate for Mo_6S_8 and $M_2Mo_6S_8$ (M = Fe, Mn, and Cu) electrocatalysts; (e) HER performance for the catalysts in Ar-saturated electrolyte; (f) The mechanism for N_2 absorption and subsequent conversion to NH_3 on $Fe_2Mo_6S_8$ [74].

Faraday Efficiency (FE) of 12.5% and an average rate of 70 μg h^{-1} mg_{cat}^{-1} for NH_3 production at −0.20 V vs RHE as displayed in Fig. 4(d–f). The mechanism can be described in Fig. 4 (f) as Fe/Mo sites contribute to N_2 adsorption and activation. Fe in $Fe_2Mo_6S_8$ suppresses competing hydrogen precipitation reactions. $Fe_2Mo_6S_8$ provides the best activity and selectivity for NRR [74]. As $Fe_2Mo_6S_8$ provide the best performance for NRR, lately, the mechanism has been investigated with computational method based on grand-canonical density functional theory (GC-DFT). It is revealed that the Fe sites of $Fe_2Mo_6S_8$ selectively stabilizes the key *NNH intermediate by the narrow band of free-atom-like surface d-states, which destroy the NRR scale relationship. The GC-DFT method can be widely applied to seek stable catalysts [76]. Most of the performance in Chevrel phase catalyst have been summarized in Table 3. Meanwhile, A remarkable characteristic of CPs which contain mixed-metal clusters is their catalytical activity to reduce molecular oxygen electrochemically to water under acid environment. The composition of $Mo_{4.2}Ru_{1.8}Se_8$ showed catalytic activity comparable to platinum [77]. The electrocatalytic oxygen reduction reaction (ORR) can be carried out by a $2e^-$ pathway that converts to H_2O_2 or a $4e^-$ pathway that converts to H_2O. Recently, $Ni_2Mo_6S_8$ was used to adjust the electrocatalytic oxygen reduction. It has a high efficiency H_2O_2 production with over 90% molar selectivity at a wide potential range and a high yielding rate of ≈90 mmol H_2O_2 g_{cat}^{-1} h^{-1} despite its very low surface area. The protruding activity is due to the ligand and the systematic effect of Ni which promote the reaction of H_2O dissociation and the proton bond of O_2 to HOO* = . The spatial effect of the CPs' structure which suppresses O–O decomposition by separating the Ni active sites and the Ni active sites is included [78]. This work provided new opportunities to look for earth-abundant catalysts.

Table 3
Summary of performance in Chevrel phase catalyst.

Material	*j* (mV)	Current density (mA/cm^2)	Tafel slope ($mV\ dec^{-1}$)	Catalytic type	Ref.
$NiMo_3S_4$	257	10	121	HER	67
Mo_6S_8	320	10	67	HER	68
$K_2Mo_6S_6$	270	10	51.9	HER	69
Mo_6S_8	321	10	74	HER	70
Mo_6Se_8	432	10	81	HER	70
Mo_6Te_8	634	10	77	HER	70
Nano Mo_6S_8	230	10	72	HER	71
Mo_6S_8@C	232	10	82	HER	72
$CuMo_6S_8$/Cu	172	10	43	HER	73
$Cu_2Mo_6S_8$	400	35	–	CO_2RR	74
$FeMo_6S_8$	200	0.5	170	NRR	75

5. Conclusions and outlook

We summarized the crystal structure characteristic, synthesis methods, and electrochemical properties of Chevrel phase compounds to provide a baseline from which future studies can be built upon. Chevrel compounds with the properties of facile metal ion intercalation, tunable crystal and electronic structures, and high stability, enables the use as rechargeable battery electrodes and electro-catalysts. The electrochemical properties of Chevrel compounds can be useful in a broad range of applications, specifically cathode materials and catalysis technologies of current interests. To guide the future investigation on Chevrel compounds, an outlook is provided as follows:

(1) As electrode materials, Chevrel compounds can be feasible for other multi-electron transfer battery systems from studying their structure and performance correlation.
(2) Electro-catalytic performance may be further improved by tuning the 3d transition metals or doping with other effective catalytic metal in Chevrel compounds.
(3) The investigation of Chevrel compounds can be more effective by combining in situ or operando characterizations and theoretical methods.
(4) Large-scale synthetic methods for nanoscale CPs with lower power consumption, shorter time are needed, such as Joule heating and improved microwave assisted method.

Author contributions

Meng Liu and Guocheng Lv wrote the manuscript. Tianming Liu,

Lintao Tian and Lingchang Kong participated in spell checking and grammar checking. Libing Liao and Juchen Guo revised the manuscript. All authors reviewed the manuscript.

Additional information

Correspondence and requests for materials should be addressed to G.L.

Declaration of competing interest

The authors declare that they have no known competing financial interests or personal relationships that could have appeared to influence the work reported in this paper.

Acknowledgments

This work was supported by the National Natural Science Foundation of China (No. 21875223). J.G. acknowledges the support from the U.S. National Science Foundation through grant CBET-1751929.

References

[1] F. Wang, J.D. Haridintwali, Z.Z. Yuan, M. Wang, F. Wang, S. Li, Z.G. Yin, L. Huang, Y.H. Fu, L. Li, S.X. Chang, L.J. Zhang, J. Rinklebe, Z.Q. Yuan, Q.G. Zhu, L.L. Xiang, D.C.W. Tsang, L. Xu, J.M. Chen, Technologies and perspectives for achieving carbon neutrality, Innovation 2 (2021), 100180, https://doi.org/10.1016/j.xinn.2021.100180.

[2] E. Levi, Y. Gofer, Y. Vestreed, E. Lancry, D. Aurbach, A promising cathode material for new rechargeable Mg batteries: a mechanically induced chemical reaction, Chem. Mater. 14 (2002) 2767–2773, https://doi.org/10.1021/cm021122o.

[3] R. Flükiger, R. Baillif, E. Walker, Single crystals of chevrel-type compounds: growth, stoichiometry and electrical resistivity, Mater. Res. Bull. 13 (1987) 743–750, https://doi.org/10.1016/0025-5408(78)90035-1.

[4] O. Pena, Chevrel phases: past, present and future, Physica C 514 (2015) 95–112, https://doi.org/10.1016/j.physc.2015.02.019.

[5] S. Belin, L. Burel, R. Chevrel, M. Sergent, Self-molybdenum intercalation: stabilization of metastable pseudo-binary Chevrel phases in Mo_6Se_8–Mo_6S_8 system, Mater. Res. Bull. 35 (2000) 151–168, https://doi.org/10.1016/S0025-5408(00)00208-7.

[6] C. Hamard, V. Auffret, O. Pena, M.L. Floch, B. Nowak, A. Wojakowski, Chevrel-phase solid solution $Mo_6Se_{8-x}Te_x$. Study of its superconducting magnetic and NMR properties, Physica B 291 (2000) 339–349, https://doi.org/10.1016/S0921-4526(99)02286-3.

[7] P. Saha, P.H. Jampani, M.K. Datta, D. Hong, B. Gattu, P. Patel, K.S. Kadakia, A. Manivannan, P.N. Kumta, A rapid solid-state synthesis of electrochemically active Chevrel phases (Mo_6T_8; T =S, Se) for rechargeable magnesium batteries, Nano Res. 10 (2000) 1–21, https://doi.org/10.1007/s12274-017-1695-z.

[8] S. Belin, R. Chevrel, M. Sergent, Single crystal structural investigations on $Ni_yMo_6Se_{8-x}S_x$ solid solution: a new location of nickel counterions, J. Solid State Chem. 155 (2000) 250–258, https://doi.org/10.1006/jssc.2000.8961.

[9] A. Mancour-Billah, R. Chevrel, The transition element sulfo-selenide Chevrel phases: a new way to stabilize the $Mo_6(S,Se)_8$ framework, J. Alloys Compd. 383 (2004) 49–56, https://doi.org/10.1016/j.jallcom.2004.04.007.

[10] T. Caillat, J.P. Fleurial, Thermoelectric properties of the semiconducting Chevrel phase $Mo_2Re_4Se_8$, J. Phys. Chem. Solid. 59 (1998) 1139–1144, https://doi.org/10.1016/S0022-3697(97)00183-2.

[11] E. Levi, G. Gershinsky, D. Aurbach, O. Isnard, Crystallography of chevrel phases, MMo_6T_8(M = Cd, Na, Mn, and Zn, T = S, Se) and their cation mobility, Inorg. Chem. 48 (2009) 8751–8758, https://doi.org/10.1021/ic900805g.

[12] D. Aurbach, Y. Gofer, Z. Lu, A. Schechter, O. Chusid, H. Gizbar, Y. Cohen, V. Ashkenazi, M. Moshkovich, R. Turgeman, E. Levi, A short review on the comparison between Li battery systems and rechargeable magnesium battery technology, J. Power Sources 97 (2001) 28–32, https://doi.org/10.1016/S0378-7753(01)00585-7.

[13] E. Levi, G. Gershinsky, D. Aurbach, O. Isnard, G. Ceder, New insight on the unusually high ionic mobility in Chevrel phases, Chem. Mater. 21 (2009) 1390–1399, https://doi.org/10.1021/cm900033v.

[14] G.S. Suresh, M.D. Levi, D. Aurbach, Effect of chalcogen substitution in mixed $Mo_6S_{8-n}Se_n$ (n = 0, 1, 2) Chevrel phases on the thermodynamics and kinetics of reversible Mg ions insertion, Electrochim. Acta 53 (2008) 3889–3896, https://doi.org/10.1016/j.electacta.2007.11.052.

[15] J. Neuhausen, E.W. Finckh, W. Tremel, $Nb_xRu_{6-x}Te_8$, new chevrel-type clusters containing niobium and ruthenium, Inorg. Chem. 35 (1996) 5622–5626, https://doi.org/10.1021/ic9508379.

[16] A. Perrin, R. Chevrel, M. Sergent, Synthesis and electrical properties of new chalcogenide compounds containing mixed (Mo, Me)$_6$ octahedral clusters (Me= Ru or Rh), J. Solid State Chem. 33 (1980) 43–47, https://doi.org/10.1016/0022-4596(80)90547-2.

[17] R. Chevrel, M. Sergent, J. Prigent, Sur de nouvelles phases sulfurées ternaires du molybdène, J. Solid State Chem. 3 (1971) 515–519, https://doi.org/10.1016/0022-4596(71)90095-8.

[18] C. Hamard, V. Auffret, O. Pena, M.L. Floch, B. Nowak, A. Wojakowski, Chevrel-phase solid solution $Mo_6Se_{8-x}Te_x$. Study of its superconducting magnetic and NMR properties, Physica B 291 (2000) 339–349, https://doi.org/10.1016/S0921-4526(99)02286-3.

[19] N.R. Singstock, J.C. Ortiz-Rodríguez, J.T. Perryman, C. Sutton, J.M. Velazquez, C.B. Musgrave, Machine learning guided synthesis of multinary chevrel phase chalcogenides, J. Am. Chem. Soc. 143 (2021) 9113–9122, https://doi.org/10.1021/jacs.1c02971.

[20] R. Flükiger, R. Baillif, E. Walker, Single crystals of chevrel-type compounds: growth, stoichiometry and electrical resistivity, Mater. Res. Bull. 13 (1978) 743–750, https://doi.org/10.1016/0025-5408(78)90035-1.

[21] E. Levi, Y. Gofer, Y. Vestfreed, E. Lancry, D. Aurbach, $Cu_2Mo_6S_8$ chevrel phase, A promising cathode material for new rechargeable Mg batteries: a mechanically induced chemical reaction, Chem. Mater. 14 (2002) 2767–2773, https://doi.org/10.1021/cm021122o.

[22] M.A. Mcguire, C. Ranjan, F.J. Disalvo, $Cu_4Mo_6Se_8$: synthesis, crystal structure, and electronic structure of a new chevrel phase structure type, Inorg. Chem. 45 (2006) 2718–2726, https://doi.org/10.1021/ic052013p.

[23] G. Gershinsky, O. Haik, G. Salitra, J. Grinblat, E. Levi, G.D. Nessim, E. Zinigrad, D. Aurbach, Ultra-fast elemental synthesis of high yield copper chevrel phase with high electrochemical performance, J. Solid State Chem. 188 (2012) 50–58, https://doi.org/10.1016/j.jssc.2012.01.016.

[24] E. Levi, E. Lancry, A. Mitelman, D. Aurbach, G. Ceder, D. Morgan, O. Isnard, Phase diagram of Mg insertion into chevrel phases, $Mg_xMo_6T_8$ (T: S, Se). 2. The crystal structure of triclinic $MgMo_6Se_8$, Chem. Mater. 18 (2006) 3705–3714, https://doi.org/10.1021/cm061656f.

[25] G. Concas, F. Congiu, A.G. Lehmann, C. Muntoni, S. Sanna, G. Spano, Magnetic susceptibility of the cluster compounds Mo_6Se_8 and Mo_6Te_8, Z. Naturforsch. 57 (2002) 221–225, https://doi.org/10.1515/zna-2002-0503.

[26] P. Saha, P.H. Jampani, M.K. Datta, C.U. Okoli, A. Manivannan, P.N. Kumta, A convenient approach to Mo_6S_8 chevrel phase cathode for rechargeable magnesium battery, J. Electrochem. Soc. 161 (2014) A593–A598, https://doi.org/10.1149/2.061404jes.

[27] K.S. Nanjundaswamy, N.Y. Vasanthacharya, J. Gopalakrishnan, C.N.R. Rao, Convenient synthesis of the chevrel phases $M_xMo_6S_8$ (M: Cu, Pb, La, or Gd), Inorg. Chem. 26 (1987) 4286–4288, https://doi.org/10.1021/ic00272a028.

[28] Y.W. Cheng, L.L. Luo, L. Zhong, J.Z. Chen, B. Li, W. Wang, S.X. Mao, C.M. Wang, V.L. Sprenkle, G.S. Li, J. Liu, Highly reversible zinc-ion intercalation into chevrel phase Mo_6S_8 nanocubes and applications for advanced zinc-ion batteries, ACS Appl. Mater. Interfaces 8 (2016), 13673, https://doi.org/10.1021/acsami.6b03197.

[29] M. Rabiller-Baudry, M. Sergent, R. Chevrel, Convenient syntheses of Chevrel phase compounds from soluble sulfide precursors under flowing hydrogen atmosphere, Mater. Res. Bull. 26 (1991) 519–526, https://doi.org/10.1016/0025-5408(91)90192-O.

[30] E. Lancry, E. Levi, A. Mitelman, S. Malovany, D. Aurbach, Molten salt synthesis (MSS) of $Cu_2Mo_6S_8$-New way for large-scale production of Chevrel phases, J. Solid State Chem. 179 (2006) 1879–1882, https://doi.org/10.1016/j.jssc.2006.02.032.

[31] M.L. Mao, Z.J. Lin, Y.X. Tong, J.M. Yue, C.L. Zhao, J.Z. Lu, Q.H. Zhang, L. Gu, L.M. Suo, Y.S. Hu, H. Li, X.J. Huang, L.Q. Chen, Iodine vapor transport-triggered preferential growth of chevrel Mo_6S_8 nanosheets for advanced multivalent batteries, ACS Nano 14 (2020) 1102–1110, https://doi.org/10.1021/acsnano.9b08848.

[32] S.H. Choi, J.S. Kim, S.G. Woo, W. Cho, S.Y. Chio, J. Chio, K.T. Lee, M.S. Park, Y.J. Kim, Role of Cu in Mo_6S_8 and Cu mixture cathodes for magnesium ion batteries, ACS Appl. Mater. Interfaces 7 (2015) 7016–7024, https://doi.org/10.1021/am508702j.

[33] D. Aurbach, G.S. Suresh, E. Levi, A. Mitelman, O. Mizrahi, O. Chusid, M. Brunelli, Progress in rechargeable magnesium battery technology, Adv. Mater. 19 (2007) 4260–4267, https://doi.org/10.1002/adma.200701495.

[34] F. Murgia, P. Antitomaso, L. Stievano, L. Monconduit, R. Berthelot, Express and low-cost microwave synthesis of the ternary chevrel phase $Cu_2Mo_6S_8$ for application in rechargeable magnesium batteries, J. Solid State Chem. 242 (2016) 151–154, https://doi.org/10.1016/j.jssc.2016.07.022.

[35] M. Furuyama, N. Kobayashi, Y. Muto, Electron-phonon interactions in the superconducting Chevrel phase compounds $Mo_6Se_{8-x}S_x$, Physiol. Res. B. 40 (1989) 4434, https://doi.org/10.1103/PhysRevB.40.4344.

[36] S. Belin, R. Chevrel, M. Sergent, Single crystal structural investigations on $Ni_yMo_6Se_{8-x}S_x$ solid solution: a new location of nickel counterions, J. Solid State Chem. 155 (2000) 250–258, https://doi.org/10.1006/jssc.2000.8961.

[37] M.B. Abdellatif, G. Patrick, L. General, Y.P. Jean, S. Marcel, R. Chevrel, New type-structure of Chevrel Phase: unusual location of the 3d chromium ions in the Mo_6Se_8 host lattice, Corat. Chem. Acta. 68 (1995) 891–899. https://hrcak.srce.hr/136701.

[38] A. Mancour-Billah, R. Chevrel, A new increasing delocalization of M =3d-elements (Ti, Fe, Co) in the channels network of the ternary $M_yMo_6Se_8$ Chevrel phases, J. Solid State Chem. 170 (2003) 281–288, https://doi.org/10.1016/S0022-4596(02)00086-5.

[39] E. Lancry, E. Levi, Y. Gofer, M. Levi, G. Salitra, D. Aurbach, Leaching chemistry and the performance of the Mo_6S_8 cathodes in rechargeable Mg batteries, Chem. Mater. 35 (2004) 2832–2838, https://doi.org/10.1021/cm034944+.

[40] W.H. Wang, L. Shi, D. Lan, Q. Li, Improving cycle stability of SnS anode for sodium-ion batteries by limiting Sn agglomeration, J. Power Sources 377 (2018) 1–6, https://doi.org/10.1016/j.jpowsour.2017.11.084.

[41] Y.C. Du, Z.Z. Zhang, Y.F. Xu, J.C. Bao, X.S. Zhou, Metal sulfide-based potassium-ion battery anodes: storage mechanisms and synthesis strategies, Acta Phys. Chim. Sin. 28 (2022) 1–14. http://doi:10.3866/PKU.WHXB202205017.

[42] M. Nagao, H. Kitaura, A. Hayashi, M. Tatsumisago, High rate performance, wide temperature operation and long cyclability of all-solid-state rechargeable lithium batteries using Mo-S chevrel-phase compound, J. Electrochem. Soc. 160 (2013) A819, https://doi.org/10.1149/2.058306jes.

[43] K. Lu, S.Y. Gao, R.J. Dick, Z. Sattar, Y.W. Cheng, A fast and stable Li metal anode incorporating an Mo_6S_8 artificial interphase with super Li-ion conductivity, J. Mater. Chem. A. 7 (2019) 6038–6044, https://doi.org/10.1039/C8TA12450G.

[44] P. Jaumaux, X. Yang, B. Zhang, J. Safaei, X. Tang, D. Zhou, C.S. Wang, G.X. Wang, Localized water-in-salt electrolyte for aqueous lithium-ion batteries, Angew. Chem., Int. Ed. 60 (2021) 19965–19973, https://doi.org/10.1002/anie.202107389.

[45] F. Malchik, N. Shpigel, M.D. Levi, T.S. Mathis, A. Mor, Y. Gogotsi, D. Aurbach, Superfast high-energy storage hybrid device composed of MXene and Chevrel-phase electrodes operated in saturated LiCl electrolyte solution, J. Mater. Chem. A. 7 (2019) 19761–19773, https://doi.org/10.1039/C9TA08066J.

[46] A. Elgendy, A.A. Papaderakis, R. Cai, K. Polus, S.J. Haigh, A.S. Walton, D.J. Lewis, R.A.W. Dryfe, Nanocubes of Mo_6S_8 Chevrel phase as active electrode material for aqueous lithium-ion batteries, Nanoscale 14 (2022) 10125–10135, https://doi.org/10.1039/D2NR02014A.

[47] P.F. Yu, Y.J. Xia, X.F. Feng, S. Zheng, G.X. Ren, N. Zhang, X.S. Liu, C. Chen, X.X. Guo, The evolution of local structure of Mo_6S_8 during Li^+ electrochemical storage studied by in-situ tender X-ray absorption spectroscopy, Prog. Nat. Sci-Mater. (2022), https://doi.org/10.1016/j.pnsc.2022.09.006.

[48] J. Yue, X.Y. Zhu, F.D. Han, X.L. Fan, L.N. Wang, J. Yang, C.S. Wang, Long cycle life all-solid-state sodium ion battery, ACS Appl. Mater. Interfaces 10 (2018) 39645–39650, https://doi.org/10.1021/acsami.8b12610.

[49] K. Lu, S. Gao, G. Li, J. Kaelin, Z.C. Zhang, Y.W. Cheng, Regulating interfacial Na-ion flux via artificial layers with fast ionic conductivity for stable and high-rate Na metal batteries, Mater. Lett. 1 (2019) 303–309, https://doi.org/10.1021/acsmaterialslett.9b00257.

[50] D. Aurbach, Z. Lu, A. Schechter, Y. Gofer, H. Gizbar, R. Turgeman, Y. Cohen, M. Moshkovich, E. Levi, Prototype systems for rechargeable magnesium batteries, Nature 407 (2000) 724–727, https://doi.org/10.1038/35037553.

[51] D. Muthuraj, S. Mitra, Reversible Mg insertion into chevrel phase Mo_6S_8 cathode: preparation, electrochemistry and X-ray photoelectron spectroscopy study, Mater. Res. Bull. 101 (2018) 167–174, https://doi.org/10.1016/j.materresbull.2018.01.031.

[52] P.F. Yu, X.H. Long, N. Zhang, X.F. Feng, J.M. Fu, S. Zheng, G.X. Ren, Z. Liu, C. Wang, X.S. Liu, Charge distribution on S and intercluster bond evolution in Mo_6S_8 during the electrochemical insertion of small cations studied by X-ray absorption spectroscopy, J. Phys. Chem. Lett. 10 (2019) 1159–1166, https://doi.org/10.1021/acs.jpclett.8b03622.

[53] L.K. Chellappan, J. Kvello, J.R. Tolchard, P.I. Dahl, S.M. Hanetho, R. Berthelot, A. Fiksdahl, K. Jayasayee, Non-nucleophilic electrolyte based on ionic liquid and magnesium bis (diisopropyl) amide for rechargeable magnesium-ion batteries, ACS Appl. Energy Mater. 3 (2020) 9585–9593, https://doi.org/10.1021/acsaem.0c01026.

[54] R. Attias, M.S. Chae, B. Dlugatch, M. Oliel, D. Aurbach, The role of surface adsorbed Cl^- complexes in rechargeable magnesium batteries, ACS Catal. 10 (2020) 7773–7784, https://doi.org/10.1021/acscatal.0c01956.

[55] L. Wang, P. Jankowski, C. Njel, W. Bauer, Z.Y. Li, Z. Meng, B. Dasari, T. Vegge, J.M.G. Lastra, Z.Z. Karger, M. Fichtner, Dual role of Mo_6S_8 in polysulfide conversion and shuttle for Mg-S batteries, Adv. Sci. 9 (2022), 2104605, https://doi.org/10.1002/advs.202104605.

[56] G.S. Kang, S. Li, S.V. Bhoraskar, J.B. Yoo, Effect of the crystalline structure of $Cu_xMo_6S_8$ on the capacity of Mg-based secondary batteries, ACS Appl. Energy Mater. 5 (2022) 8346–8356, https://doi.org/10.1021/acsaem.2c00899.

[57] X. Qu, A. Du, T. Wang, Q.Y. Kong, G.D. Chen, Z.H. Zhang, J.W. Zhao, X. Liu, X.H. Zhou, S.M. Dong, G.L. Cui, Charge-compensation in a displacement Mg^{2+} storage cathode through polyselenide-mediated anion redox, Angew 61 (2022), e202204423, https://doi.org/10.1002/anie.202204423.

[58] P.W. Wang, J. Truck, J. Hacker, A. Schlosser, K. Kuster, U. Starke, L. Reinders, M.R. Buchmeiser, A design concept for halogen-free Mg^{2+}/Li^+-dual salt-containing gel-polymer-electrolytes for rechargeable magnesium batteries, Energy Storage Mater. 49 (2022) 509–517, https://doi.org/10.1016/j.ensm.2022.04.034.

[59] W.J. Zhao, Y.J. Zhang, H.M. Li, K.L. Wang, K. Jiang, Large-scale fabricating carbon coating Chevrel phase in molten salts: implications for high-performance magnesium-ion battery cathode, J. Alloys Compd. 925 (2022), 166745, https://doi.org/10.1016/j.jallcom.2022.166745.

[60] T.M. Liu, G.C. Lv, M. Liu, C.C. Zhao, L.B. Liao, H. Liu, J.Y. Shi, J. Zhang, J.C. Guo, Cation-intercalation and conversion-type cathode materials for rechargeable aluminum batteries, Mater. Chem. Front. 3 (2022) 280–296, https://doi.org/10.1039/D1QM01267C.

[61] L. Geng, G.C. Lv, X.B. Xing, J.C. Guo, Reversible electrochemical intercalation of aluminum in Mo_6S_8, Chem. Mater. 27 (2015) 4926–4929, https://doi.org/10.1021/acs.chemmater.5b01918.

[62] L. Geng, J.P. Scheifers, J.P. Zhang, K.N. Bozhilov, J.C. Guo, Crystal structure transformation in Chevrel phase Mo_6S_8 induced by aluminum intercalation, Chem. Mater. 30 (2018) 8420–8425, https://doi.org/10.1021/acs.chemmater.8b03312.

[63] Y.X. Tong, A. Gao, Q.H. Zhang, T. Gao, J.M. Yue, F.Q. Meng, Y. Gong, S.B. Xi, Z.J. Lin, M.L. Mao, S.Y. Peng, X.F. Wang, D.D. Xiao, D. Su, Y.H. Luo, H. Li, L.Q. Chen, L.M. Suo, L. Gu, Cation-synergy stabilizing anion redox of Chevrel phase Mo_6S_8 in aluminum ion battery, Energy Storage Mater. 37 (2021) 87–93, https://doi.org/10.1016/j.ensm.2021.01.033.

[64] X.Y. Wen, Y.H. Liu, A. Jadhav, J. Zhang, D. Borchardt, J.Y. Shi, B.M. Wong, B. Sanyal, R.J. Messinger, J.C. Guo, Materials compatibility in rechargeable aluminum batteries: chemical and electrochemical properties between vanadium pentoxide and chloroaluminate ionic liquids, Chem. Mater. 31 (2019) 7238–7247, https://doi.org/10.1021/acs.chemmater.9b01556.

[65] A.L. Jadhav, J.H. Xu, R.J. Messinger, Quantitative molecular-level understanding of electrochemical aluminum-ion intercalation into a crystalline battery electrode, ACS Energy Lett. 5 (2020) 2842–2848, https://doi.org/10.1021/acsenergylett.0c01138.

[66] M.L. Agiorgousis, Y.Y. Sun, D. West, S.B. Zhang, Intercalated Chevrel phase Mo_6S_8 as a Janus material for energy generation and storage, ACS Appl. Energy Mater. 1 (2018) 440–446, https://doi.org/10.1021/acsaem.7b00092.

[67] J. Jiang, P. Gao, W. Sheng, Y.S. Yan, Hollow chevrel-phase $NiMo_3S_4$ for hydrogen evolution in alkaline electrolytes, Angew 128 (2016) 1–6, https://doi.org/10.1002/ange.201607651.

[68] K.M. Naik, S. Sampath, Cubic Mo_6S_8-efficient electrocatalyst towards hydrogen evolution over wide pH range, Electrochim. Acta 252 (2017) 408–415, https://doi.org/10.1016/j.electacta.2017.09.015.

[69] J.T. Perryman, A.T. Kulkarni, J.M. Velázquez, Direct solid-state nucleation and charge-transport dynamics of alkali metal-intercalated $M_2Mo_6S_6$ (M= K, Rb, Cs) nanorods, J. Mater. Chem. C 8 (2020) 10742–10748, https://doi.org/10.1039/D0TC01674H.

[70] J.C. Ortiz-Rodríguez, N.R. Singstock, J.T. Perryman, F.P. Hyler, J.M. Velazquez, Stabilizing hydrogen adsorption through theory-guided chalcogen substitution in Chevrel-phase Mo_6X_8 (X= S, Se, Te) electrocatalysts, ACS Appl. Mater. Interfaces 12 (2020) 35995–36003. http://10.1021/acsami.0c07207.

[71] J. Strachan, A.F. Masters, T. Maschmeyer, Chevrel phase nanoparticles as electrocatalysts for hydrogen evolution, ACS Appl. Nano Mater. 4 (2021) 2030–2036, https://doi.org/10.1021/acsanm.0c03355.

[72] A. Elgendy, A.A. Papaderakis, C. Byrne, Z.Z. Sun, J.V. Lauritsen, E.P.C. Higgins, A. Ejigu, R. Cernik, A.S. Walton, D.J. Lewis, R.A.W. Dryfe, Nanoscale chevrel-phase Mo_6S_8 prepared by a molecular precursor approach for highly efficient electrocatalysis of the hydrogen evolution reaction in acidic media, ACS Appl. Energy Mater. 4 (2021) 13015–13026, https://doi.org/10.1021/acsaem.1c02646.

[73] H.M. Liu, R.K. Xie, Y.T. Luo, Z.C. Cui, Q.M. Yu, Z.Q. Gao, Z.Y. Zhang, F.N. Yang, X. Kang, S.Y. Ge, S.H. Li, X.F. Gao, G.L. Chai, L. Liu, B.L. Liu, Dual interfacial engineering of a Chevrel phase electrode material for stable hydrogen evolution at 2500 mA cm^{-2}, Nat. Commun. 13 (2022) 1–10, https://doi.org/10.1038/s41467-022-34121-y.

[74] K. Lu, F. Xia, B.M. Li, Y.Z. Liu, I.B.A. Razak, S.Y. Gao, J. Kaelin, D.E. Brown, Y.W. Cheng, Synergistic multisites $Fe_2Mo_6S_8$ electrocatalysts for ambient nitrogen conversion to ammonia, ACS Nano 15 (2021) 16887–16895, https://doi.org/10.1021/acsnano.1c07771.

[75] J.T. Perryman, J.C. Ortiz-Rodríguez, J.W. Jude, F.P. Hyler, R.C. Davis, A. Mehta, A.R. Kulkarni, C.J. Patridge, J.M. Velazquez, Metal-promoted Mo_6S_8 clusters: a platform for probing ensemble effects on the electrochemical conversion of CO_2 and CO to methanol, Mater. Horiz. 7 (2020) 193–202, https://doi.org/10.1039/C9MH00745H.

[76] N.R. Singstock, C.B. Musgrave, How the bioinspired $Fe_2Mo_6S_8$ chevrel breaks electrocatalytic nitrogen reduction scaling relations, J. Am. Chem. Soc. 144 (2022) 12800–12806, https://doi.org/10.1021/jacs.2c03661.

[77] J. Neuhausen, E.W. Finckh, W. Tremel, New chevrel-type clusters containing niobium and ruthenium, Inorg. Chem. 35 (1996) 5622–5626, https://doi.org/10.1021/ic9508379.

[78] F. Xia, B. Liu, Y. Liu, Y. Liu, S.Y. Gao, K. Lu, J. Kaelin, R.Y. Wang, T.J. Marks, Y.W. Cheng, Carbon free and noble metal free $Ni_2Mo_6S_8$ electrocatalyst for selective electrosynthesis of H_2O_2, Adv. Funct. Mater. 31 (2021), 2104716, https://doi.org/10.1002/adfm.202104716.